Liquid Flow Analysis in the Evaporator Grooves of the Cold Plate

Han Hwangbo* and W. S. McEver*
MRJ, Subsidiary of Perkin-Elmer Corporation, Oakton, Virginia

An analytical model of a two-phase cold-plate operation is developed. The model describes the liquid flows in the evaporator grooves to identify the factors limiting thermal performance. It is found that the liquid-carrying components are crucial to the overall performance of the device. In particular, the evaporator groove geometry is important. Grooves with a rectangular cross section are found to be capable of handling much larger liquid flow rates (and thus higher power levels) than V-shaped grooves. Grooves with a large aspect ratio (depth to width) provide better performance than shallower grooves. An optimum groove width is found to give the maximum power handling capability of the cold plate.

Nomenclature

A = cross-sectional area of liquid under meniscus in groove
$\bar{A}$ = dimensionless cross-sectional area, $= A/W^2$
a_0, a_1 = constants
D_h = hydraulic diameter of groove, $= 4A/Pm$
$\bar{D}_h$ = dimensionless hydraulic diameter of groove, $= D_h/W$
f = fanning friction factor, $= K/R_e$
H = groove depth
h_{fg} = latent heat of vaporization
K = dimensionless constant
L = length of the groove
L_w = length of communication wick
N = number of grooves per unit length
P_o = permeability
p = fluid pressure
Pm = wetted perimeter of groove $(2H + 2W)$
q = heat flux density
R = radius of curvature
Re = Reynolds number
v = velocity
W = groove half-width
z = coordinate along the groove
α = meniscus contact angle
μ = viscosity of fluid
ρ = density of fluid
σ = surface tension force

Subscripts

h = hydraulic
ℓ = liquid
r = reservoir
v = vapor
w = wick

Superscript

$-$ = dimensionless quantity

Presented as Paper 85-0921 at the AIAA 20th Thermophysics Conference, Williamsburg, VA, June 19-21, 1985; received July 23, 1986; revision received Aug. 26, 1987.

*Member, Technical Staff.

Introduction

A COLD-PLATE (CP) is a heat exchanger designed to remove heat from electronic units. Cold plates presently used in space applications use a single-phase fluid (water or Freon-21). Excess heat is removed as the fluid increases in temperature flowing through the CP. In a two-phase system, the fluid boils or evaporates as it passes through the cold plate. The excess heat does not appear as a fluid temperature rise but as an increase in the percentage of the fluid that is converted into vapor.

A schematic of the cold plate is shown in Fig. 1. In the CP mode, liquid flows from the reservoir through the wick to the evaporator grooves. Heat is conducted from the heat sources (an electronics unit, for example) through the wall of the cold plate to the tip of the capillary grooves, where the liquid evaporates. The liquid flow continues along the evaporator grooves as liquid is vaporized. The vapor flows out of the CP to a separate condenser, where the heat is rejected. As the liquid level in the reservoir drops, it is periodically replenished by opening a valve in the liquid supply line.

Some of the theory developed for heat pipes[1] is applicable to the present study because of the similarity of the CP to a heat pipe. However, there are several major differences between the CP and a heat pipe, the most important one being the way liquid is supplied to the two devices. In a heat pipe, liquid is transported from the condenser section to the evaporator through the action of capillary forces. This liquid flow is countercurrent to the vapor flow. The CP, on the other hand, receives its liquid from a separate condenser via a pumped liquid supply line. Also, for the case considered here, the vapor flow is at right angles to liquid flow. As a consequence, the CP does not have the performance limitations characteristic of a heat pipe, and heat pipe performance studies are not directly applicable to the CP. Consequently, our analytical efforts were directed to identifying performance limiting features of the CP and the design tradeoffs.

Evaporator Groove

Consider a capillary groove as shown in Fig. 2. The pressure of the liquid is given by

$$p_\ell = p_v - \sigma/R \tag{1}$$

where σ is the surface tension of the liquid, R the radius of curvature of the meniscus, and p_v the vapor pressure. The radius of curvature may be written in terms of the groove half-width W and the contact angle of the meniscus with the

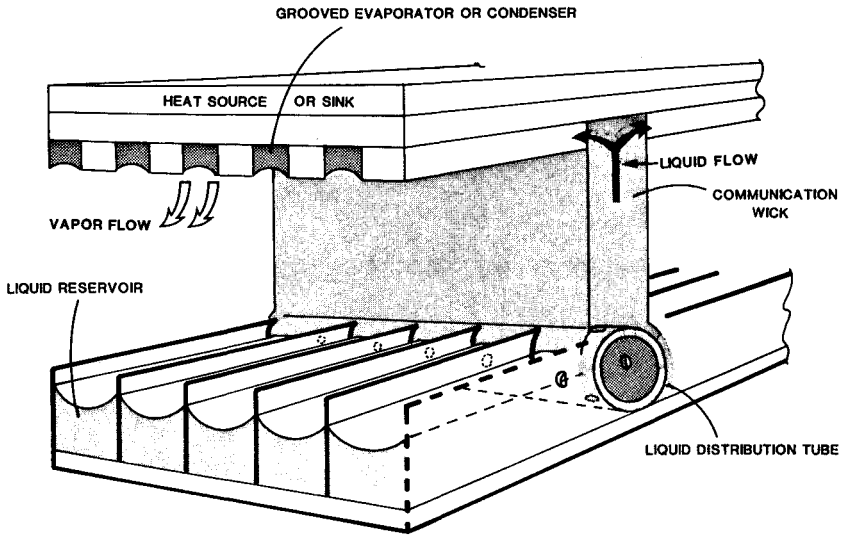

Fig. 1 Schematic of cold plate.

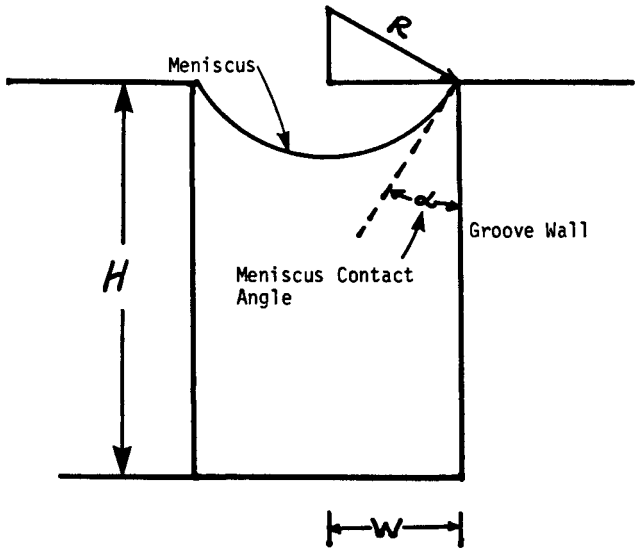

Fig. 2 Capillary groove geometry.

groove wall,

$$R = W/\cos\alpha \tag{2}$$

Substituting Eq. (2) into Eq. (1) and differentiating with respect to the coordinate along the groove z, we have

$$\frac{dp}{dz} = \frac{\sigma}{W}\sin\alpha\,\frac{d\alpha}{dz} \tag{3}$$

where we have assumed $dp_v/dz = 0$, i.e., the change in vapor pressure along the groove length is very small since the grooves run at right angles to the vapor flow. We have also dropped the subscript ℓ in Eq. (3). In the following equations, all physical properties are those of the liquid state, and all geometric parameters refer to the groove unless otherwise noted.

The change in pressure drop down the groove resulting from viscous losses is customarily written

$$\frac{dp}{dz} = -\frac{f}{D_h}\left(\frac{\rho v^2}{2}\right) \tag{4}$$

where v is the average liquid velocity in the groove and D_h is the groove hydraulic diameter. For an open channel such as the groove, D_h is defined as

$$D_h = \frac{4A}{P_m} \tag{5}$$

with A being the flow cross-sectional area of the groove (area defined by the groove walls and liquid meniscus) and P_m the wetted perimeter of the groove $(2H + 2W)$.

For laminar flow within the groove, the Fanning friction factor f may be written as

$$f = K/Re \tag{6}$$

where the friction coefficient K is dimensionless and $Re = \rho v D_h/\mu$.

If N is the number of grooves per unit width of the cold plate, L the groove length, and q the heat flux density, then, $q(L/N)$ is the total heat flux absorbed by a single groove.

At any point z along the length of the groove, the heat flux that will be carried off by the remainder of the groove is $q[(L - z)/N]$. This must be matched by the product of the mass flow rate times latent heat of vaporization, i.e.,

$$\dot{m}h_{fg} = q\,\frac{(L - z)}{N} \tag{7}$$

since $\dot{m} = \rho v A$, we have

$$v = \frac{q(L - z)}{\rho h_{fg} A N} \tag{8}$$

where ρ is the liquid density and h_{fg} the latent heat of vaporization. The average velocity is a maximum at the start of the groove ($z = 0$) and zero at the groove end. In Eq. (8), we have made the assumption that the heat input is uniform along the length of the groove.

Since the flow down the groove in 0 g is driven only by capillary forces, the pressure loss given by Eq. (4) must be compensated for by a change in contact angle given by Eq. (3). Setting Eqs. (3) and (4) equal and using Eqs. (7) and (8), we have

$$\frac{d\alpha}{dz} = -\left(\frac{\mu}{\rho\sigma h_{fg}}\right)\left(\frac{KW^4}{2D_h^2 A}\right)\frac{q(L - z)}{NW^3\sin\alpha}$$

$$= -\left(\frac{\mu}{\rho\sigma h_{fg}}\right)\left(\frac{K}{2\bar{D}_h^2 A}\right)^*\frac{q(L - z)}{NW^3\sin\alpha} \tag{9}$$

The * in Eq. (9) denotes a dimensionless parameter. We have used the groove half-width W to make $\bar{D}_h^2\bar{A}$ nondimensional.

The term $(K/(2\bar{D}_h^2\bar{A}))^*$ is a function of α and the groove aspect ratio (ratio of depth to width, $H/2W$). In Appendix A, we present the results of a numerical analysis to determine this relationship. Equation (9) is separable into terms depending only on α and z and may thus be integrated. From Appendix A, we use the following relationship:

$$(2\bar{D}_h^2\bar{A}/K)^* = a_0 + a_1\alpha \tag{10}$$

for the dependence of the geometric factor on contact angle. The constants a_0, a_1 depend on groove aspect ratio and are tabulated in Appendix A.

Substituting Eq. (10) into Eq. (9) and integrating from $\alpha = \alpha_0$ to α_1, ($z = 0$ to $z = L$) and solving for q, we have

$$q = \left(\frac{\rho a h_{fg}}{\mu}\right)\frac{2W^3N}{L^2}\left\{a_0(\cos\alpha_1 - \cos\alpha_0) - a_1\left[(\sin\alpha_1 - \alpha_1\cos\alpha_1) - (\sin\alpha_0 - \alpha_0\cos\alpha_0)\right]\right\} \tag{11}$$

Equation (11) cannot be solved explicitly for q because α_0 is a function of q, as is seen in the next section.

Communication Wick

The pressure drop in the communication wick ΔP_w is given by

$$\Delta P_w = \frac{\mu}{\rho}\frac{L_w\dot{m}}{P_o A_w} \tag{12}$$

where L_w is the wick length, A_w the wick cross-sectional area, and $\dot{m}$ the liquid mass flow rate. Po is a wick parameter called the permeability. Generally, Po must be determined experimentally from pressure drop measurements and Eq. (12).

The mass flow rate is proportional to the heat flux density times the groove length. Equation (12) may be rewritten

$$\frac{\Delta P_w}{qL} = \frac{\mu}{\rho h_{fg}}\frac{L_w}{tPo} \tag{13}$$

where L_w is the distance along the wick from the liquid level in the reservoir to the evaporator grooves and t is the wick half-thickness. These are depicted in Fig. 3. The term $\Delta p_w/qL$ is the product of a liquid physical properties term and a wick properties term and is a constant for a given liquid and wick.

The pressure drop in the wick establishes the meniscus contact angle at the beginning of the evaporator groove α_0. This is illustrated schematically in Fig. 4. If we assume that the radius of curvature of the meniscus in the reservoir is much larger than in the evaporator grooves, then, from Eqs. (1) and (2), we have

$$\cos\alpha_0 = \frac{W}{\sigma}(\Delta P_w/qL)qL \tag{14}$$

where $(\Delta P_w/qL)$ is given by Eq. (13). Thus, for a given fluid and wick, α_0 is determined by the groove half-width W, groove length L, and heat flux density q. Since $0\text{ deg} < \alpha_0 < 90$ deg, the relationship between q, W, and L is

$$WqL < \sigma/(\Delta P_w/qL) \tag{15}$$

Liquid Reservoir Wick

The purpose of the liquid reservoir wick is to stabilize and contain the liquid in a 0-g environment and deliver it to the communication wick. In addition, the reservoir wick should be capable of withstanding the pressure differential created by the vapor flow. The liquid/vapor pressure differential is given by Eq. (1). If ΔP_v is the vapor pressure drop in the vapor space above reservoir, then,

$$\Delta P_v \leq \frac{\sigma}{R_r} \tag{16}$$

where R_r is the minimum radius of curvature of the meniscus in the reservoir.

For a reservoir wick composed of parallel plates with spacing d, the minimum value of R_r is $d/2$. This sets an upper limit on the allowable vapor pressure drop.

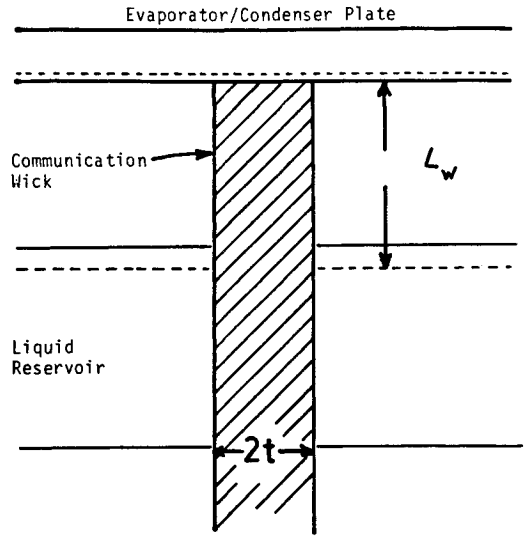

Fig. 3 Wick geometry.

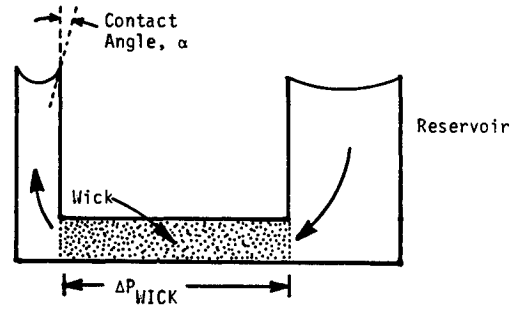

Fig. 4 Relationship between wick ΔP and meniscus contact angle.

Cold-Plate Heat-Transfer Coefficient

It is known from analyses of grooved heat pipes that the primary mode of evaporator heat transfer is from the cold-plate wall through the metal fin between the grooves to a thin film of liquid where the meniscus contacts the groove wall. Almost all the resistance to heat transfer takes place at this point and is due primarily to the thermal resistance of the liquid layer. Since the flow in this layer is laminar, convective effects are small, and the heat-transfer coefficient can be calculated based on conductive heat flow from the wall of the groove through the liquid film to the meniscus surface. The liquid evaporates from the surface that is at the saturation temperature of the vapor.

In the study by Schneider and Yovanovich,[2] a finite-element thermal model of the groove/meniscus was developed. Their results showed a very high heat-transfer coefficient that was largely independent of the meniscus contact angle. In the paper by Kamotani,[3] an analytical model was used for large contact angles and a finite-difference numerical model was used for small contact angles. Kamotani's results for the

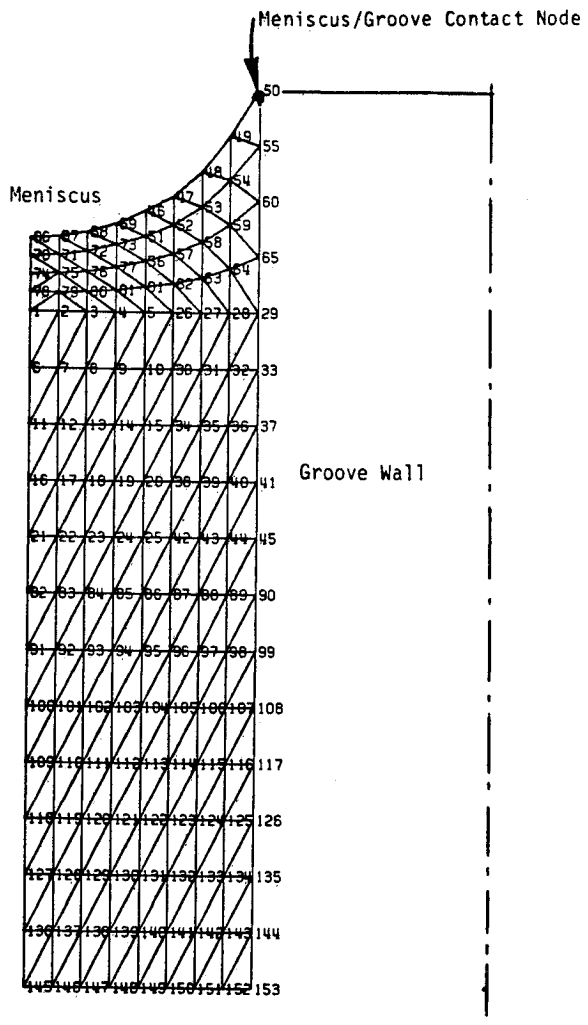

Fig. 5 Finite-element grid for groove hydraulic model.

groove heat-transfer coefficient were considerably smaller than those found by Schneider and Yovanovich (S-Y) and showed a large dependence on contact angle.

A large dependence of heat-transfer coefficient on α will partially invalidate our groove liquid flow model, which contained the assumption of uniform evaporation rate down the length of the groove with α changing continuously down the tube.

We attempted to duplicate the studies by constructing a finite-element thermal model of a liquid-filled groove. The element grid is shown in Fig. 5. Note that only half of the groove is modeled because of symmetry about the groove centerline.

Several runs were made with a constant-temperature difference between the bottom of the groove and the meniscus surface. The total heat flow through the groove varied significantly depending on how the node at the intersection of the meniscus and groove wall was specified. If the node temperature was fixed at the constant meniscus temperature, a very large heat flow passed through the tip of the groove at that node. Assuming a finite resistance between the metal tip and the fluid node at the interface resulted in a much lower heat flow. In the S-Y model, there was a similar effect. Schneider and Yovanovich attempted to mitigate the effect of this singular point on the heat flow by using a very large number of nodes. Even with this fine subdivision, approximately one-half of the total heat flow was through the node at the meniscus/wall contact point.

Accurate prediction of the heat-transfer rate in the evaporator groove by using the finite-element modeling technique requires a good knowledge of the thermal resistance between the meniscus and the wall based on experiment. The determination of thermal conductances of the thin liquid film attached to the groove wall has been the subject of recent studies.[4-6]

It is reported in a test at a uniform heat flux of 4 W/cm^2 that the heat-transfer coefficients of narrow-groove cold plate (aspect ratio = 5, depth/width = 0.064/0.0127 cm) fell in a range of 0.66-0.88 W/cm^2/°C with $R - 11$.[7] The grooved heat pipes have average heat-transfer coefficients in the range of 0.5-1.4 W/cm^2/°C for the Freons. With the optimized grooves (aspect ratio = 3, depth/width = 0.150/0.050 cm) at 4 W/cm^2, the cold plate is expected to have thermal performance similar to the grooved heat pipes.

Cold-Plate Design

In the preceding section, the theoretical background of the CP was presented. In this section, the theory is used to design the CP and to estimate its performance. There were two performance requirements established for the CP. One was the capability to handle power densities up to 4 W/cm^2 applied uniformly to the plate. The other requirement concerns cold-plate outlet quality. Quality is defined as the ratio of the mass flow rate that is vapor to the total flow rate. A quality of 1 (or 100%) corresponds to a flow of saturated vapor only. With outlet qualities close to 100%, the total thermal bus flow rate will be minimized, as well as the toal pressure drop in the system. Furthermore, high quality minimizes the uncertainties associated with two-phase pressure drop correlations and thus increases confidence in overall system design. Based on these considerations, an outlet quality at least 90% was established as a design goal.

In the following sections, design calculations are presented based on the use of Freon-11 as the working fluid. Freon-11 is relatively nontoxic and has the advantage of a boiling point at room temperature. Its thermodynamic properties are somewhat inferior to those of ammonia, so that a design based on Freon-11 will have better performance when used with ammonia.

Communication Wick Design

As discussed earlier, the communication wick pressure drop establishes the contact angle between the meniscus and the groove wall. The term $\Delta P_w/qL$ given by Eq. (13) was evaluated for a wick with a length of 2 cm (the vapor channel height), a thickness of 0.5 cm, and permeability of 8×10^{-10}m^2. This permeability corresponds to that of fairly porous sintered metal mesh or a mesh composed of metal screens. These wick parameters result in a value of 1×10^{-2} Pa/W – m for $\Delta\rho/qL$, using Freon-11 physical properties.

Groove Dimensions

In the theoretical section, Eq. (11) was derived giving the maximum heat-flux density q, that a groove can handle in terms of the groove geometry and physical properties of the liquid. Since the initial contact angle α_0 also depends on q through Eq. (14), we cannot solve Eq. (11) explicitly for q.

A solution to Eq. (11) was obtained using the root determination program RTMI, which is part of the Scientific Subroutine Package installed on the VAX 11/780 computer used for the study. Equation (11) was simplified by assuming that the groove land area (area at top of groove) was equal to the groove root area. In this case, the number of grooves per unit length N is given by $1/4W$, where W is the groove half-width. The communication wick factor was held constant at 1×10^{-2} Pa/W – m. This factor is required for calculation of the initial meniscus contact angle. The final contact angle was set at 10 deg. This is somewhat conservative assumption since for wetting liquids, such as the Freons, the contact angle will approach 0 deg.

Solutions were obtained for Eq. (11) are plotted as q vs the total groove width ($2W$) with the groove length as a

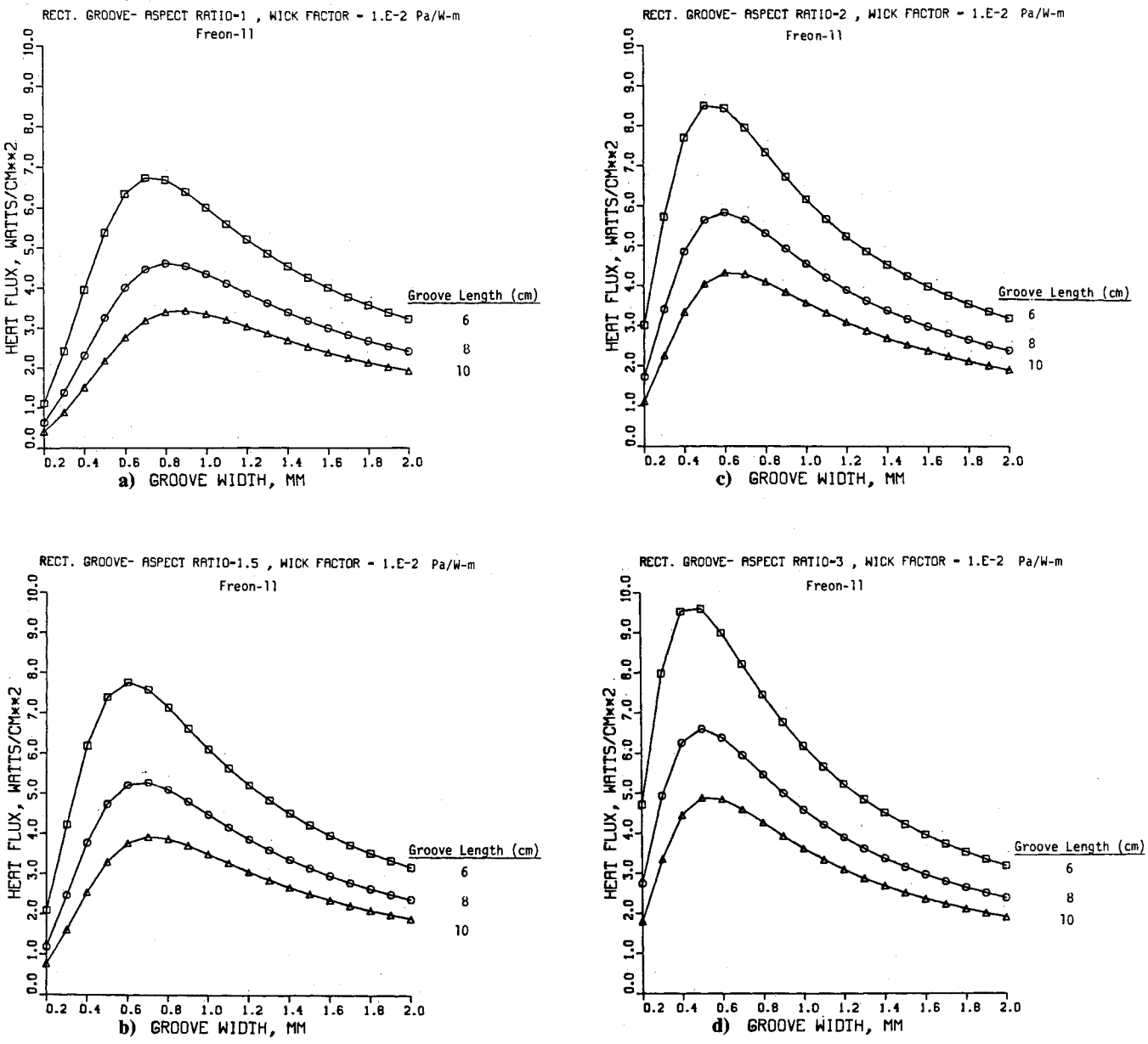

Fig. 6 Maximum heat flux vs groove width.

parameter. The solutions were performed for rectangular groove aspect ratios (ratio of groove depth to groove width) of 1, 1.5, 2, and 3. These plots are presented in Figs. 6a–6d. Figure 7 is the same plot for a 60-deg V-groove. As can be seen from inspection of the figures, the rectangular grooves have a much greater heat flux capability than the V-groove. This is due to the superior hydraulic characteristics of rectangular grooves. Grooves with large aspect ratios also show larger heat handling capability for the same reason.

The most notable feature of the curves is the appearance of an optimum groove width. This optimum depends on groove length as well as aspect ratio. The maximum in the curves arises as a result of two limiting factors. At small groove widths, the viscous pressure drop restricts the amount of liquid the groove can carry. As the groove becomes wider, the hydraulic factors improve rapidly, and the maximum heat flux capability rises sharply. At some point, however, a further increase in groove width produces diminishing returns because of the effect of the communication wick pressure drop, which determines the initial meniscus/groove wall contact angle, as given by Eq. (14). In this region of groove widths, q varies inversely with W, as shown in Eq. (15).

The variation of the maximum flux with the communication wick factor dp/QL is shown in Fig. 8 for a fixed groove geometry. This shows that decreasing the pressure drop across the wick improves the heat flux capability of the groove. It should be noted that setting the pressure drop across the wick to zero (initial contact angle = 90 deg) results in a maximum heat flux capability that continually increases with groove width.

Obviously, there are many combinations of groove width, length, and aspect ratio that will meet the required heat flux density of 4 W/cm^2. Following is a discussion of some of the other factors that enter into the design process.

The entrainment limit given by a Weber number of 1 does not help in selecting the groove width.[8] All the groove widths of interest give Weber numbers very much less than 1 for an outlet vapor velocity corresponding to $q = 4$ W/cm^2, a 2-cm vapor chamber height, and 50-cm length.

Other considerations that enter into selection of groove geometry are: 1) manufacturability, 2) capability of operation with damaged grooves or wicks, and 3) 1-g testing.

Groove widths in the 0.4–0.6-mm range are about equally manufacturable in the lengths, aspect ratios, and spacing we

are considering. Maintaining a rectangular groove cross section may present some difficulties; but, as long as the walls are not too tapered, performance will not suffer appreciably.

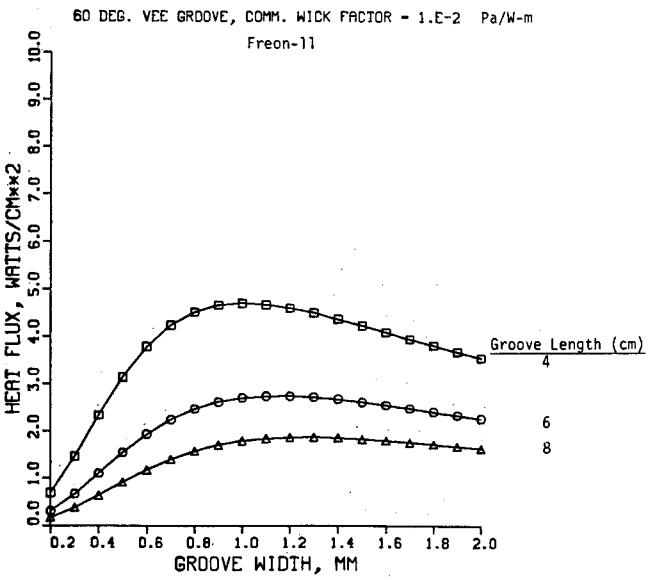

Fig. 7 Maximum heat flux vs groove width.

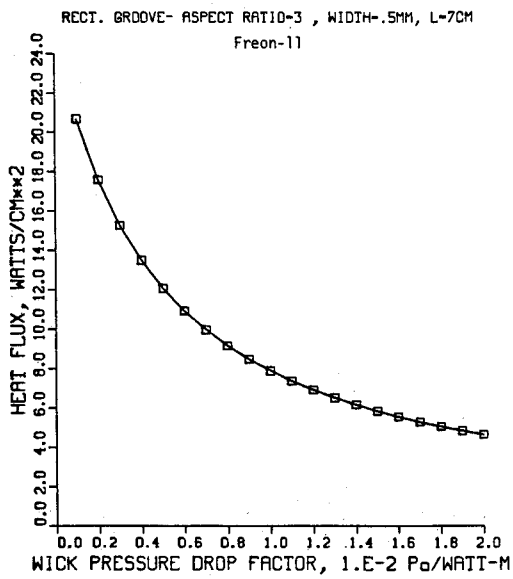

Fig. 8 Maximum heat flux vs $\Delta P_w/qL$.

The possibility of grooves becoming clogged and/or wicks damaged can be handled by overdesign so that local overloads can be accommodated. Note, from the variation of heat flux capability with aspect ratio, that some clogging or filling of the grooves can be tolerated. The effect of 1-g on cold-plate performance will be to prevent operation with groove widths in the 0.5-mm range since the capillary forces cannot overcome the gravitational head. The grooves can be kept primed if an external reservoir is used that gravity-feeds liquid to the top of the communication wick. This simulates operation at 0-g.

Based on the preceding discussion, the following groove parameters have been selected for our prototype: 1) width, 0.5 mm; 2) length, 7 cm; and 3) depth, 1.5 mm (aspect ratio = 3). These parameters give a theoretical performance much higher than the design requirement (factor of 2). The 7-cm groove

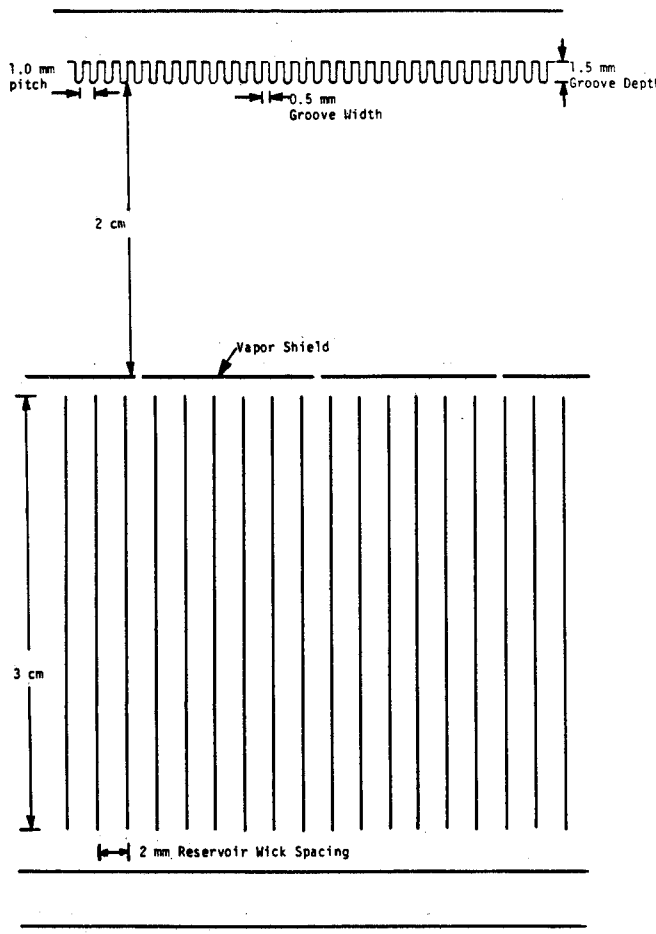

Fig. 10 Cold-plate cross section showing groove and reservoir geometry.

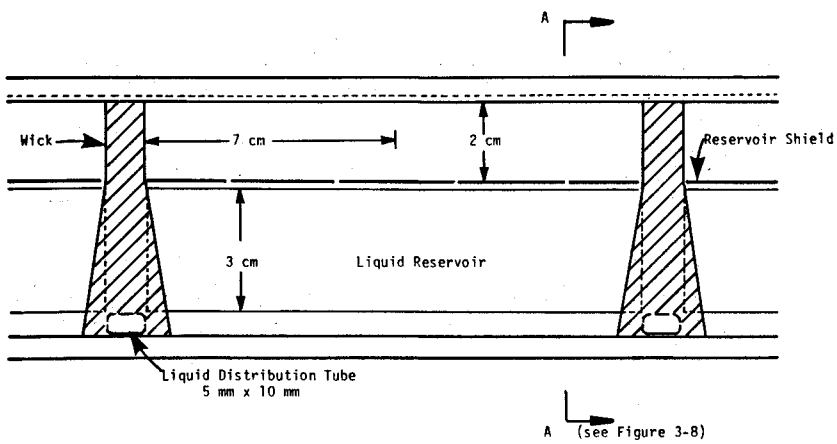

Fig. 9 Cold-plate details.

length was selected to accommodate the 70-mm bolt hole spacing presently used on single-phase cooled cold plates. The actual location and integration of the mechanical fasteners into the CP have not been considered in the present study.

Design Summary

Figure 9 illustrates a cross section of the prototype CP, with the direction of vapor flow normal to the paper. The 7-cm groove length results in a 14-cm vapor chamber width. The factor of 2 performance margin ensures liquid supply to the groove at the design heat flux, even with one wick inoperative. A small gap below the reservoir wick fin provides a low-pressure drop path for liquid level equalization during operation with nonuniform heat loads. The wicks and distribution tubes also provide flow paths for reservoir equalization.

In Fig. 10, the groove and reservoir wick cross sections are shown. A rounded groove tip geometry is used to give high heat-transfer coefficients at all meniscus contact angles.

Conclusions

An analytical model of cold-plate operation was developed. The modeling effort concentrated on describing the liquid flows to identify the factors limiting thermal performance. It was determined that the liquid-carrying components were crucial to the overall performance of the device. In particular, it was found tht evaporator groove geometry was important. Grooves with a rectangular cross section were found to be capable of handling much larger liquid flow rates (and thus higher power levels) than V-shaped grooves. Grooves with a large aspect ratio (ratio of depth to width) provided better performance than shallower grooves although the dependence of maximum power density on aspect ratio was not strong.

The key parameter for the evaporator grooves was the groove width. With all other parameters fixed, the maximum power handling density vs groove width curve gave a broad maximum. The occurrence of an optimum groove width is due to two factors. At narrow groove widths, the groove is incapable of carrying sufficient liquid because of the high viscous pressure drop down the length of the groove. For very wide grooves, the capillary pressure head developed by the groove (inversely proportional to groove width) is insufficient to make up for the pressure drop experienced in the wick. In other words, the wick acts as a flow restrictor. However, there is ample margin in all the parameters to enable a cold plate to be designed to meet the power density requirement of 4 W/cm^2. Vapor chamber size and reservoir dimensions were chosen to minimize pressure gradients and entrainment of the liquid in the vapor stream. This will assume high outlet qualities for the device.

Acknowledgments

The work reported in this paper was supported by NASA under Contract NAS9-17029. The authors acknowledge the technical advice of Paul Marshall and Gary Rankin of NASA Johnson Space Center.

Appendix: Liquid Flow in a Rectangular Capillary Groove

As liquid flows down the rectangular capillary grooves in the cold-plate evaporator surface, the pressure drops because of viscous shear with the wall of the groove. Since the flow is in an open channel exposed to the vapor and there is no gravitational force (0-g), the pressure loss must be made up as a decrease in the radius of curvature of the liquid meniscus. In order to calculate how much liquid flow a groove can carry for a given groove length and heat flux, it is necessary to have an accurate knowledge of the viscous pressure losses. It is well known that approximations using the hydraulic diameter and circular tube friction factors can be seriously in error for laminar flow.

Ayyaswamy et al.[9] studied the similar problem of capillary flow in triangular grooves. They determined the friction factor coefficient K, which is defined in terms of the friction factor $f = K/Re$, with the Reynolds number Re calculated using the hydraulic diameter of the groove. For circular pipes, K has a value of 64. For triangular grooves, Ayyaswamy and coworkers found that K varied with groove half-angle and meniscus contact angle. The overall range of K was approximately 55–30. Thus, it can be seen that use of the conventional laminar flow friction factor and the hydraulic diameter would give a factor of 2 error for certain combinations of the groove half-angle and contact angle. Kamotani[3] used a similar approach for a rectangular groove except that an approximate function was used that did not satisfy the boundary conditions at all points. Furthermore, only a limited range of groove geometries was considered.

The procedure we used is similar in concept to that used by Ayyaswamy et al., except that the rectangular groove geometry we studied made the solutions to the governing flow equations and their boundary conditions more difficult. This will be discussed.

With the usual assumptions of steady laminar flow of an incompressible Newtonian fluid in a groove aligned with the z axis, we may write the equation of motion immediately from the Navier-Stokes equations as

$$\nabla^2 v = \frac{\partial^2 v}{\partial x^2} + \frac{\partial^2 v}{\partial y^2} = \frac{1}{\mu}\frac{dp}{dz}$$

where v is the velocity in the z direction and μ the dynamic viscosity. We may make the above equation dimensionless by the following normalizations:

$$\bar{x} = \frac{x}{W} \qquad \bar{y} = \frac{y}{W} \qquad \bar{v} = \frac{v}{(W^2/\mu)(dp/dz)}$$

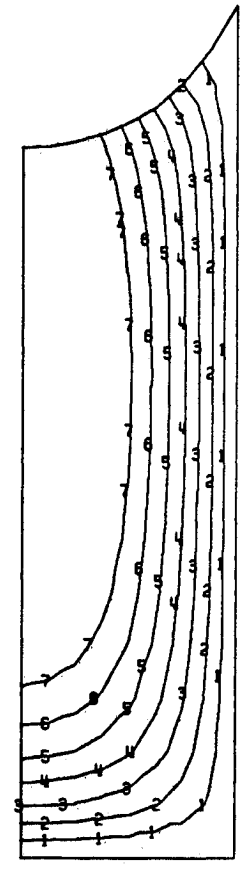

Fig. A1 Isovelocity contours for capillary groove.

Then, we have

$$\bar{\nabla}^2 \bar{v} = 1$$

which is recognized as Poisson's equation.

The boundary conditions are that the velocity is zero at the walls of the groove (the no-slip condition) and that the normal derivative of the velocity is zero at the meniscus surface. In Ref. 9, an analytical solution for the above equation was obtained in cylindrical coordinates with the no-slip boundary condition. The normal derivative boundary condition was handled using the Galerkin boundary method. In the case of rectangular coordinates, there is no exact analytical solution to Poisson's equations for any of the boundary conditions.

In the present study, we adopted a numerical approach to the solution of the equation. A numerical solution can be obtained using either finite-difference or finite-element methods. The finite-element method was considered superior for our geometry and boundary conditions since a zero normal derivative on the curved meniscus surface is easily handled by use of finite elements. This type of boundary condition, on the other hand, is very difficult to handle accurately with the finite-difference method.

The NASTRAN finite-element code was used to generate solutions to Poisson's equation with the rectangular geometry and boundary conditions just discussed. Since NASTRAN does not have a general-purpose partial differential solution procedure, we used a thermal analogy to the preceding equation. The thermal equivalent to the groove flow problem is a thin rectangular plate that has one curved side (corresponding to the meniscus). The curved side is insulated (normal derivative of temperature = 0). The other three sides are held at a fixed temperature of zero (corresponding to $v = 0$). The plate has a uniform heat flux generated through the interior of the plate.

The plate temperatures generated by NASTRAN for the temperature equivalent of our fluid flow problem correspond to contours of fluid velocities. In Fig. 5, the finite-element grid is shown for one of the cases analyzed. Figure A1 shows the isotherms contours. Note that, because of symmetry, only half of the groove is modeled. From the temperature at each node, the average temperature was calculated and used to calculate an overall average using the areas of the individual finite elements as weighting factors. This average temperature was appropriately normalized to give the dimensionless average velocity in the groove.

Several checks were made on the accuracy of this procedure. In one case, an approximate analytical solution to Poisson's equation was obtained in a square using a series of harmonic polynomials, with coefficients determined by a boundary colocation method. The finite-element technique gave results within 2% of the analytical method using a relatively coarse grid such as that shown in Fig. 5. In another test case, a triangular groove was modeled. The average velocity was within 0.8% of the result obtained by Ayyaswamy et al. with their analytical technique.

Once the average dimensionless velocity $\langle \bar{v} \rangle$ is determined from the NASTRAN solution, the friction factor coefficient may be determined as follows:

$$\frac{dp}{dz} = \frac{K \rho v^2}{Re D_h^2}$$

$$Re = \frac{\rho v D_h}{\mu}$$

$$K = \frac{2D_h^2 (dp/dz)}{\mu V} = \frac{2\bar{D}_h^2}{\langle \bar{v} \rangle}$$

where $\bar{D}_h$ is the dimensionless hydraulic diameter (normalized by the groove half-width w).

A series of runs were made for meniscus contact angles from 0 to 90 deg and aspect ratios (depth to width) of 1, 1.5, 2, and 3. The theory developed in Eq. (9) of this paper made use of a groove hydraulic factor $(2\bar{D}_h^2 \bar{A})/K$, where $\bar{A}$ is the dimensionless groove cross-section area $\bar{A} = A/W^2$.

Using the above definition of K, we find that $(2\bar{D}_h^2 \bar{A})/K = \bar{v}\bar{A}$, which is the dimensionless volumetric flow rate in the groove.

The quantity $\bar{v}\bar{A}$ could be accurately fit by the linear equation $a_0 + a_1\alpha$, where α is the meniscus contact angle in radians. Values of a_0 and a_1 are presented in Table A1.

Table A1 Hydraulic factor coefficients

Aspect ratio	a_0	a_1
1	0.3128	0.3789
1.5	0.9186	0.4204
2	1.574	0.4245
3	2.990	0.3424

References

[1]Dunn, P.D. and Reay, D.A., *Heat Pipes,* Pergammon Press, Oxford, England, 1976.

[2]Schneider, G.E. and Yovanovich, M., "Thermal Analysis of Trapezoidal Grooved Heat Pipe Walls," Research Institute Report, University of Waterloo, Ontario, Canada, Project 3061-2, 1975.

[3]Kamotani, Y., "Thermal Analysis of Axial Grooved Heat Pipes," *Proceedings of the 2nd International Heat Pipe Conference,* Bologna, Italy, European Space Agency, 1976, p. 83.

[4]Renk, F.C. and Wayner, P.C. Jr., "An Evaporating Ethanol Meniscus, Part I," *ASME Journal of Heat Transfer,* Vol. 101, Feb. 1979, p. 55.

[5]Renk, F.C. and Wayner, P.C. Jr., "An Evaporating Ethanol Meniscus, Part II," *ASME Journal of Heat Transfer,* Vol. 101, Feb. 1979, p. 59.

[6]Holm, F.W. and Goplen, S.P., "Heat Transfer in the Meniscus Thin-Film Transition Region," *ASME Journal of Heat Transfer*, Vol. 101, Aug. 1979, p. 543.

[7]Grote, M.G. and Swanson, T.D., "Design and Testing of a Pumped Two-Phase Mounting Plate," AIAA Paper 85-0919, June 1985.

[8]Hwangbo, H. and McEver, W.S., "High Thermal Capacity Hot Plate/Cold Plate," Final Report to NASA under Contract NAS9-17029, May 31, 1984.

[9]Ayyaswamy, P.S., Catton, I., and Edwards, D.K., "Capillary Flow in Triangular Grooves," *Journal of Applied Mechanics,* June 1974, p. 332.